Characterization of Film Formation from Direct Mini-emulsified Polystyrene Latex Particles via SANS

K. D. Kim,[†,‡,§] L. H. Sperling,*[,†,‡,§,∥] and A. Klein[†,§,⊥]

Polymer Interfaces Center, Center for Polymer Science and Engineering, Materials Research Center, Department of Chemical Engineering, Department of Materials Science and Engineering, and Emulsion Polymer Institute, Whitaker Laboratory #5, Lehigh University, Bethlehem, Pennsylvania 18015

G. D. Wignall

Solid State Division, Oak Ridge National Laboratory, Oak Ridge, Tennessee 37830

Received August 25, 1992; Revised Manuscript Received May 3, 1993

ABSTRACT: Mini-emulsified latexes of anionically polymerized deuterated and protonated polystyrene (DPS = 185 000, HPS = 200 000) were prepared by direct mini-emulsification. Films containing 6% deuterated particles were annealed at 144 °C for various periods of time. The average depth of penetration of the deuterated polystyrene chains and tensile strength buildup were characterized during the course of annealing. When the present results were compared with those of the conventional emulsion polymerized system, the directly mini-emulsified latex had greater interdiffusion rates and higher tensile strength than the emulsion polymerized latex system at similar annealing times. This difference may be due to the polydisperse nature of the molecular weight distribution and/or to the large and polar chain end groups of the emulsion polymerized system. The present system shows a minimum depth of penetration for full tensile strength of around 105–115 Å, comparable to 0.81 times the weight-average radius of gyration, R_g^w, of the whole polystyrene chain, while the tensile strength buildup was dependent on the annealing time to the 0.51 ± 0.05 power. The tensile strength curve as a function of annealing time goes through a maximum and then levels off. Finally, the diffusion coefficient from the SANS data was $(4.7 \pm 1.0) \times 10^{-16}$ cm²/s at the scattering vector $Q = 0.0067$ Å^{-1}.

Introduction

Interdiffusion of polymers is employed in a wide range of applications, including film formation, adhesion and welding between polymeric materials, crack healing, and polymer blending. Considerable development has been made in understanding polymer–polymer interdiffusion behavior, and several theories[1-6] have been proposed based on de Gennes' reptation model.[7]

Recently, studies[8-13] on the interdiffusion of polymer chains between neighboring latex particles during the process of film formation from latexes have been carried out by using small-angle neutron scattering (SANS). The advantage of using latexes stems from their very large surface area. Obviously, this is also a very practical system.

Hahn et al.[8,9] studied the interdiffusion of deuterated and protonated *n*-butyl methacrylate copolymer latex particles during the course of film formation via SANS. They found an apparent increase of the radius of gyration of the deuterated particles during the annealing process and concluded that the coalescence of the latex particles was due to a center-of-mass interdiffusion of polymer chains. At almost the same time, Anderson et al.[11] obtained the diffusion coefficient of different molecular weight pairs of deuterated/protonated polystyrene latex particles during the annealing of latex films. Especially, they prepared latexes of anionically polymerized deuterated and protonated polystyrenes by using a direct emulsification technique. However, their particle size distribution was broad.

In diffusion studies at Lehigh University, Linne et al.[10] and Yoo et al.[12,13] investigated the mechanical strength of polystyrene latex films, correlating the results with those of SANS. Latex film formation can be considered as a special case of crack healing or polymer welding. In both cases, strength development depends on polymer chain interdiffusion. Yoo et al.[12,13] investigated the relationship between tensile strength buildup and the actual depth of penetration in latex films using low and high molecular weight polystyrenes (M_w = 250 000 and 2 080 000, respectively). They found that tensile strength was fully developed at a penetration depth comparable to the weight-average radius of gyration of the whole polystyrene chain in the lower molecular weight system. Also, it was found that the interface healing theory of Wool et al.[17,18] for a flat surface could be applied to film formation from latex particles, with tensile strength buildup proportional to time raised to the one-fourth power.

It is very interesting to compare SANS results with those from other methods. Winnik et al.[14-16] used direct nonradiative energy transfer (DET) measurements (a form of fluorescence) to measure polymer diffusion during the course of latex film formation. Poly(butyl methacrylate) (PBMA) and poly(methyl methacrylate) (PMMA) latex particles were labeled with donor and acceptor groups, and the particle fusion was detected by measurements of fluorescence decay. They obtained the diffusion coefficient and correlated this with the diffusion of polymer molecules across the particle–particle boundary.

Wool et al.[17-21] have extensively studied the healing of polymer interfaces, developing the minor chain reptation model. Besides his theory, Prager and Tirrell[22-25] described the interface healing behavior with different chain end positions. According to their theory, uniform chain end distributions throughout the bulk and excess chain ends at the initial interfaces yielded a half and one-fourth power time dependence of mechanical properties, respectively.

† Polymer Interfaces Center and Center for Polymer Science and Engineering.
‡ Materials Research Center.
§ Department of Chemical Engineering.
∥ Department of Materials Science and Engineering.
⊥ Emulsion Polymer Institute.

0024-9297/93/2226-4624$04.00/0

The most fundamental assumption of the diffusion theories is the uniformity of chain length. Although Yoo et al.'s[12,13] result showed an important relationship between mechanical strength and interpenetration depth, the effect of a broad molecular weight distribution on interdiffusion reduced the accuracy of the results. For example, a broad molecular weight distribution may induce some smearing effects in the analysis of the SANS data.

In the present research, an improved direct mini-emulsification technique was used to prepare artificial latexes having both narrow molecular weight distributions and good particle size uniformity. The direct emulsified latexes have two differences from conventional emulsion polymerized latex. First, a conventional latex has ionic end groups (generally sulfates) which are mostly on the particle surface, while the chain ends of anionic polymerized polystyrene have hydrogen chain ends, and these ends will be randomly distributed in the latex particle. Second, the narrow molecular weight and particle size distributions will both be very helpful in analyzing the SANS data. In this paper, partly annealed latex films made from direct mini-emulsified, anionically polymerized polystyrene were analyzed via SANS and their tensile strengths determined for comparison.

Theoretical Background

de Gennes' reptation theory describes the diffusive motion of entangled chains. Generally, chain interdiffusion can be characterized by numerous factors, such as the diffusion coefficient, the average chain interpenetration depth, the number of bridges crossing the interface, and the fracture stress. Theoretical models have been proposed to describe the time and molecular weight dependence of each property during the course of interface healing. These models will be briefly introduced and compared.

First of all, the effect of chain length on the diffusion coefficient, D, was predicted from theories of polymer chain dynamics in concentrated solutions and melts.[1,2,4,5] The reptation model estimates that

$$D = k_d M^{-2} \tag{1}$$

where k_d is the diffusion constant and M is the molecular weight. Although some research[26,27] has shown deviation from an inverse square dependence of molecular weight, most diffusion experiments have verified the relationship.

The fracture stress, K_{IC}, was described in several models[17,18,22-25] with regard to crack healing. There is general agreement among the models that, during the course of interface healing, strength increases with time to the one-fourth power, that is

$$K_{IC} \propto t^{1/4} M^{-r/4} \tag{2}$$

where $r = 1$ or 3, and t represents the healing or annealing time. At short times, Prager and Tirrell[22-24] also predicted that the fracture stress depends on time to the one-eighth power when the contacting surfaces contain many chain ends. In this paper, tensile strength is assumed to be proportional to K_{IC}.

The average chain interpenetration depth, $d(t)$, was initially calculated by de Gennes[7] and then by Kim and Wool,[18]

$$d(t) \propto t^{1/4} M^{-1/4} \quad (t < \tau) \tag{3}$$

$$d(t) \propto t^{1/2} M^{-1} \quad (t > \tau) \tag{4}$$

where τ represents the relaxation time.

The number of bridges per unit area, $N(t)$, is defined as the number of segments of polymer chain crossing through a unit area of interface[22-24,28] which are bounded at both ends with entanglements. According to Prager and Tirrell's[22-24] prediction, for equilibrium interfaces at short times,

$$N(t) \propto t^{1/2} M^{-2/3} \tag{5}$$

and in the case of interfaces with excess chain ends

$$N(t) \propto t^{1/4} M^{-1/4} \tag{6}$$

Wool derived a relation similar to eq 5. Although there are more factors which delineate polymer–polymer interdiffusion,[20,21,28] the present experimental results will be analyzed on the basis of the above equations.

SANS Data Analysis

Interdiffusion Penetration Depth of Polymer Chains. The penetration depth, $d(t)$, of polymer chains across particle boundaries was obtained by subtracting the original radius, $R(0)$, of the deuterated latex particles in the dispersed state from the radius, $R(t)$, of the expanding deuterated polystyrene particles:

$$d(t) = R(t) - R(0) \tag{7}$$

where t stands for annealing time. The radius of deuterated polystyrene particles was calculated from

$$R^2 = (5/3)R_g^2 \tag{8}$$

where the radius of gyration, R_g, was determined from the well-known Guinier approximation,[29]

$$\frac{d\Sigma}{d\Omega}(Q) = \frac{d\Sigma}{d\Omega}(0) \exp(-Q^2 R_g^2/3) \tag{9}$$

where $d\Sigma/d\Omega$ represents the coherent scattering cross section per unit volume of the material (in units of cm^{-1}) and is proportional to the scattered intensity per detector pixel. The quantity Q is the wave vector, equivalent to $(4\pi/\lambda)\sin(\theta/2)$, where λ and θ represent the neutron wave length and the angle of scatter, respectively. The quantity R_g can be obtained from the slope of the plot $\ln(d\Sigma/d\Omega)$-(Q) vs Q^2.

The size of the deuterated polystyrene particles, which appear to expand via interdiffusion of polymer chains among neighboring particles, is an apparent and averaged quantity because of concentration fluctuations of the deuterated polystyrene chain segments at the diffusion front. Also, the expanding deuterated particles are not perfect spheres.

Diffusion Coefficient. Binder[30] derived an equation to obtain the diffusion coefficient, based on Cook's scattering equation[31] for spinodal decomposition of metal alloys. For the case of an ideal polymer solution, Binder's equation can be written as

$$I(Q,t) = I(Q,0)\exp(-2Q^2Dt) + I(Q,\infty)[1 - \exp(-2Q^2Dt)] \tag{10}$$

where $I(Q,0)$ and $I(Q,\infty)$ are the initial and equilibrium scattering intensities, respectively, and D is the diffusion coefficient.

Recently, Summerfield and Ullman[32,33] derived an equation to obtain the diffusion coefficient from SANS data on systems composed of randomly mixed particles of protonated and deuterated polymers. They showed that $I(Q,t)$, the SANS intensity at annealing time t, can be

characterized by

$$I(Q,t) = I(Q,0)\exp(-2Q^2Dt) + I(Q,\infty)\left[1 - \alpha(0,t) - \frac{1-\beta}{1-\psi}\exp(-2Q^2Dt)\right] \quad (11)$$

where $\alpha(0,t)$ is the normalized integral of the radial correlation function, $\gamma(R,0)$, characterizing the initial configurations of the particles:

$$\alpha(0,t) = (8\pi Dt)^{-3/2}\int_0^\infty \gamma(R,0)\exp(-R^2/8DT)\,dR \quad (12)$$

where R is a radial position. Furthermore, β and ψ are defined by the relationship

$$\alpha(0,0) = \frac{\beta - \psi}{1 - \psi} \quad (13)$$

where $\psi < \beta < 1$.

In the current SANS data, $I(Q,\infty)$ is much smaller (<10%) than $I(Q,0)$, especially at low angles and short annealing times. Equations 10 and 11 are reduced to the same forms when the second term is neglected. For a particular sample and annealing time, the experimental diffusion coefficients can be determined by combining data at several different Q values and annealing times by using least-square analysis. In order to investigate Q- and t-dependent effects, the t-constant diffusion coefficient, D_t, and the Q-constant diffusion coefficient, D_q, were calculated as

$$D_t = -\frac{1}{2}\{d\ln[I(Q,t)/I(Q,0)]/dQ^2\}_t/t \quad (14)$$

$$D_q = -\frac{1}{2}\{d\ln[I(Q,t)/I(Q,0)]/dt\}_q/Q^2 \quad (15)$$

respectively.[4]

Fractal Analysis. The concept of fractal geometry is essential to the understanding of SANS curves obtained from disordered materials. Basically, all fractals show a power-law dependence of the scattered intensity, I, on the momentum transfer quantity, Q, as[34]

$$I(Q) \sim Q^{-a} \quad (16)$$

where a is the Porod exponent and can be determined in the Porod region of the scattering curve. For colloidal systems, the Porod region typically lies between $Q = 0.01$ and 0.1 Å^{-1}, and the geometric parameter, a, is related to the structure such as the fractal dimension.

For scattering from three-dimensional objects with fractal surfaces, the scattering intensity can be expressed as follows:[35-37]

$$I(Q) \sim Q^{-6+d_s} \quad (17)$$

where d_s is the surface fractal dimension. For a smooth sphere, $d_s = 2$; thus, the power-law scattering exponent should be ~4. If the surface is fractally rough, d_s lies between 2 and 3, so that the slope of the scattering curve lies between −3 and −4. When the exponent is less than −3, the system is regarded as a mass fractal object. For a mass fractal object, the scattering intensity goes as

$$I(Q) \sim Q^{-d_m} \quad (18)$$

where d_m is the mass fractal dimension, obtained directly from the power-law exponent.

Experimental Section

Direct Mini-emulsification. Polystyrene latexes containing 100% deuterated species or 100% protonated species were prepared by a direct mini-emulsification technique.[38] This method is based on a direct emulsification method described by El-Aasser et al.[41] and Vanderhoff et al.[42] and a mini-emulsion method of Tang et al.[43] Some definitions are in order here. A direct emulsification involves the dispersion of matter at the colloidal level. This has been a commercial practice for polymers for many years. A mini-emulsion utilizes one or more long-chain alcohols as cosurfactants. A microemulsion replaces the long-chain alcohols by short-chain alcohols. The thermodynamics and phase relationships of each of these systems are different. This paper utilizes an improved mini-emulsion technique, whereby relatively uniform particles of polystyrene are formed from uniform anionically polymerized polystyrenes. Anionically polymerized deuterated and protonated polystyrenes which have narrow molecular weight distributions were obtained from Pressure Chemical Co. These polystyrenes were dissolved in cyclohexane with two cosurfactants, cetyl alcohol and stearyl alcohol (Kodak Co.), as an oil phase and then mixed with an aqueous phase which contained deionized distilled (DDI) water, sodium lauryl sulfate (anionic surfactant, Fisher Scientific), and more cosurfactants, cetyl alcohol and stearyl alcohol. The recipe is shown in Table I. After applying a high mechanical shear on the crude emulsion with an ultrasonic agitator for 60 s, the latex was homogenized by passing it through a polycarbonate membrane. As seen in Table I, cosurfactants exist in both phases. This is different from typical mini-emulsion recipes. The coexistence of cosurfactants in both phases is very important in making a stable emulsion state before sonification. During all the processing, temperature was maintained at 60 °C. The cyclohexane was removed by steam distillation at 105 °C for 4 h. Gas chromatography was used to check for the absence of cyclohexane.

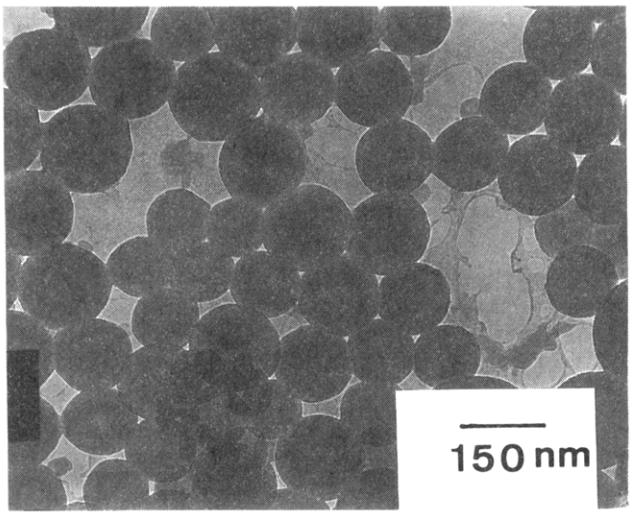

Figure 1. TEM photomicrograph of a deuterated polystyrene latex.

Table I. Direct Mini-Emulsification Recipe of Polystyrene Latexes

ingredient	weight (g)
oil phase	
polystyrene	2.0
cyclohexane	20.0
cetyl alcohol	0.256
stearyl alcohol	0.109
water phase	
water	100.0
sodium lauryl sulfate	0.435
cetyl alcohol	0.256
stearyl alcohol	0.109

Characterization. Gel permeation chromatography (Waters) was used for molecular weight determination. In addition, the results indicated that no significant breakage of the polystyrene chains occurred during the ultrasonification. The latex particle size was measured via three instruments: (1) photon correlation spectroscopy (Coulter N4MD), (2) transmission electron microscopy (TEM; Philips 400), (3) small-angle neutron scattering (Oak Ridge National Laboratory). Figure 1 represents a typical TEM photomicrograph of a dried deuterated latex. Table II

Table II. Characterization of Polystyrene Latexes

sample	M_n	M_w/M_n	particle radii (Å) TEM	SANS	Coulter
deuterated polystyrene	185 000	1.02	650	680	925
protonated polystyrene	200 000	1.05	655	700	980

summarizes the molecular weights and particle sizes of the polystyrene latexes. A polydispersity index of 1.09 was calculated for the particle sizes. The higher particle radius obtained from photon correlation spectroscopy may be due to the surfactant layer around the polystyrene latex particles. (It is noted that the present latex recipe contains a rather large amount of surfactant in comparison with a conventional emulsion polymerized latex; see below.)

Latex Binding. The deuterated latex was mixed with 14.6 times the weight of an identical protonated polystyrene latex, yielding 6 mol % of deuterated polystyrene in the mixed latex dispersion. This composition was designed to ensure that each deuterated latex particle would be surrounded primarily by protonated particles and to achieve a reasonable scattering intensity to noise ratio in the SANS experiment. After the blended latex was redried at 50 °C for 2 days, the dried powder was extracted by excess methanol for 3 days to remove the cosurfactants, followed by a hot distilled water extraction to remove the anionic surfactant, sodium lauryl sulfate. Then the cleaned latex was dried in a vacuum oven at 60 °C for 24 h. The glass transition temperature as measured by DSC (at a heating rate of 20 °C/min) was 105.9 ± 0.5 °C, in comparison with 106.6 °C for the original bulk polystyrene, indicating that nearly all of the surfactant was removed.

Sintering and Film Annealing. The dried polystyrene particles were sintered in a vacuum hot press at 110 °C for 25 min under a pressure of 10 MPa. These conditions are just sufficient to form a void-free, fully dense (see below), and transparent film, while minimizing chain interdiffusion between neighboring particles. The resulting sintered films were about 1.0 mm thick and 3.75 cm in diameter.

These bulk films were annealed at 144 °C for various times in sandwich form between two thin steel plates with a steel O-ring spacer. Thirty minutes were allowed for temperature equilibrium before the annealing time clock was started. After annealing, samples were quenched in a 15 °C water bath to inhibit further diffusion. For the SANS blank samples and tensile strength studies, 100% protonated samples were prepared by the same procedures.

The density of each sample was determined by flotation in aqueous NaCl solutions to be 1.054 ± 0.003 g/cm^3 for 6 mol % deuterated polystyrene and 1.050 ± 0.003 g/cm^3 for 100% protonated polystyrene. Since the nominal densities of protonated and deuterated polystyrene are 1.054 and 1.130 g/cm^3, respectively, the theoretical density of 6 mol % deuterated polystyrene is estimated to be 1.058 g/cm^3. Thus, it was concluded that the samples were fully dense.

SANS Measurements. The SANS experiments were performed on the 30-M SANS facility at the HFIR reactor in the Oak Ridge National Laboratory. Disk specimens with about 1.0-mm thickness and 1.3-cm diameter were used throughout the measurements. In order to measure the original size of the deuterated polystyrene latex particles in the dispersed state excluding the surfactant layer, a quartz cell having a 2-mm path length was used. A neutron wavelength of 4.75 Å ($\Delta\lambda/\lambda \sim 5\%$), the source (1.7-cm diameter), and sample slits (1.0-cm diameter) were separated by a distance of 7.5 m. The sample–detector distance was 19.1 m, and the data were corrected for instrumental background and detector efficiency on a cell-by-cell basis, prior to radial averaging to give a Q-range of $0.0033 < Q < 0.033$ Å^{-1}. The coherent intensities of the sample were obtained by subtracting the intensities of the corresponding blanks, which formed only a minor correction (<10%) to the sample data. The net intensities were converted to an absolute differential cross section by comparison with precalibrated secondary standards, based on the measurement of beam flux, vanadium incoherent cross section, the scattering from water, and other reference materials.[44]

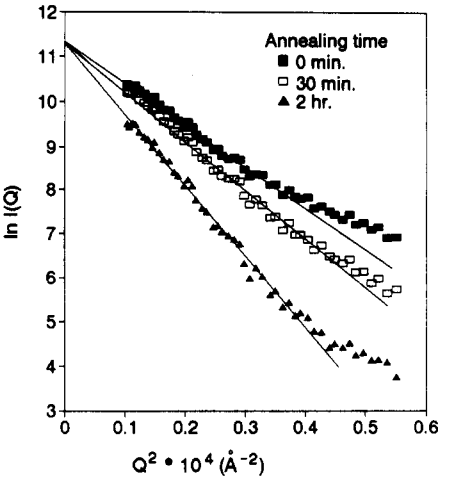

Figure 2. Determination of the deuterated polystyrene particle radius of gyration via Guinier plots.

Table III. Summary of SANS and Tensile Strength Test Results of Polystyrene Latex Films

annealing time	$R_g{}^a$ (Å)	$R_g{}^b$ (Å)	radius (Å)	average depth of penetration (Å)	tensile strength (10^5 N/m^2)
latex	527		680		
sintered	556		717		250
5 min	562		726	46	308
10 min	569		734	54	315
15 min	577		744	64	324
30 min	615		793	113	380
1 h	650		839	159	339
2 h	703		907	227	336
11 h					340
24 h	792	166			355
48 h	646	151[c]			365

[a] Determined by the Guinier approximation. [b] Obtained by the Zimm plot. [c] The relaxed random-coil dimension at infinite time is calculated to be 118 Å.

Tensile Strength Test. Micro tensile strength studies were carried out on all protonated samples at room temperature by using an Instron universal testing machine. Dumbbell-type specimens were prepared by grinding the bulk films with a fine file, followed by rubbing the ground surface with a fine sandpaper until smooth. A grip separation distance of 1.0 cm and a grip separation rate of 0.254 cm/min were employed.

Results

Guinier plots were prepared to determine the radii of gyration of the particles during the annealing process. Typical Guinier plots are shown in Figure 2 which indicate that scattering intensity decreases as annealing time increases. The results of the SANS and tensile strength data as a function of annealing time are presented in Table III. As predicted, the radius of gyration of deuterated polystyrene particles increases as annealing proceeds. In particular, the samples annealed for more than 24 h show apparent decreasing particle size because the deuterated particles start to diffuse into other deuterated particles, leaving decreasingly small clusters of deuterated chains. Therefore, Zimm plots should be applied to the data for longer annealing times as individual chain scatterings are approached.

The apparently larger R_g of the sintered particles than that of the original latex particles is attributed to interdiffusion resulting from the sintering process. The fact that there is no apparent decrease in the particle size diameter after sintering (due to anisotropy relaxation) reveals that the physical relaxation is much faster than molecular interdiffusion. This result is different from that observed in similar experiments.[8,9,12,13]

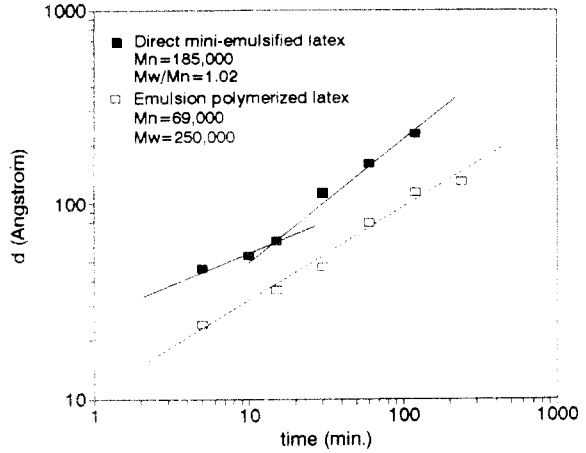

Figure 3. log–log plot of interpenetration depth, d, vs annealing time during film formation, compared with that obtained by Yoo et al.[12] The temperature of interdiffusion was 144 °C in both experiments.

In order to look at the time dependence of the average depth of penetration, a log–log plot of the interpenetration depth vs the annealing time is shown in Figure 3. By comparison, previous data from Yoo et al.'s work[12,13] for a conventional emulsion polymerized latex system (M_n = 69 000; M_w/M_n = 3.6) is plotted in the same figure. Interestingly, the direct mini-emulsification system has a much faster penetration rate than the conventional emulsion polymerization system even though its molecular weight is higher.

In the Kim and Wool model,[5] the average monomer interpenetration depth is dependent on the one-fourth power of the healing time, up to de Gennes' reptation time, when the power-law dependence changes over to the half power dependence. The expected reptation time, τ, of the current system is 9.8 min, calculated from $\tau = Nb^2/3\pi^2D^*$, where N is the degree of polymerization, b is the statistical segment length (6.7 Å for polystyrene), and D^* is the self-diffusion coefficient from SANS data. τ of Yoo et al.'s[12] conventional emulsion polymerization system is 3.7 min based on the number-average molecular weight. Thus, most of data points in Figure 3 were obtained at annealing times over the reptation time. However, in the direct mini-emulsification system, two straight line segments were obtained. The first three data points yielded a 0.29 ± 0.05 slope, which is comparable to the one-fourth power-law relationship. This power law value was shifted to a 0.57 ± 0.05 for annealing times greater than 15 min, reasonably approximating the theoretical value of 0.50.

Figure 4 represents the tensile strength buildup as a function of the average depth of penetration. This plot is also compared with the conventional emulsion polymerization system. Full tensile strength was developed at an average interpenetration depth of about 110–120 Å for both systems. Zhang and Wool[19] predicted that the maximum fracture energy occurs at the interpenetration distance, X, given by $X_\infty = 0.81\,R_g$, which predicts a value of 100 Å in the present system and 113 Å in Yoo et al.'s[12] system. However, it must be emphasized that the direct mini-emulsification system shows a somewhat higher tensile strength than films made from a conventional latex at the same interpenetration depth, especially at the low interpenetration depth.

The time dependence of tensile strength buildup is illustrated by a Wool plot in Figure 5. However, when the critical portion of the data is plotted on a log–log basis (Figure 6), it yields two slopes of 0.51 ± 0.05 and 0.32 ± 0.05. This will be discussed later. Additionally, it is

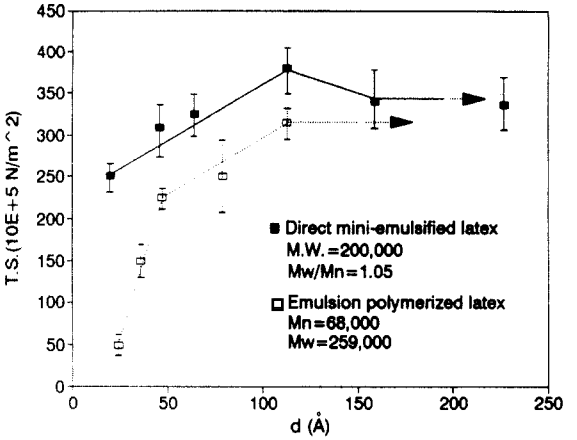

Figure 4. Tensile strength first increasing, then going through a maximum, and finally leveling off.

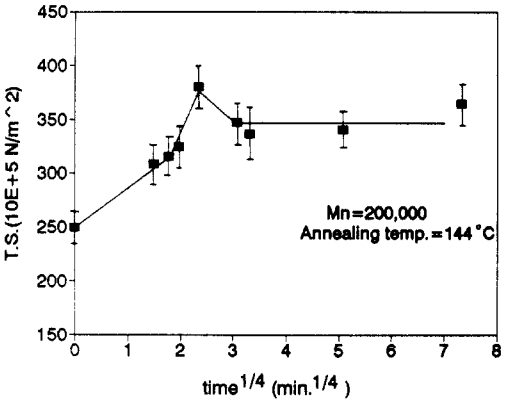

Figure 5. Wool plot shows tensile strength buildup.

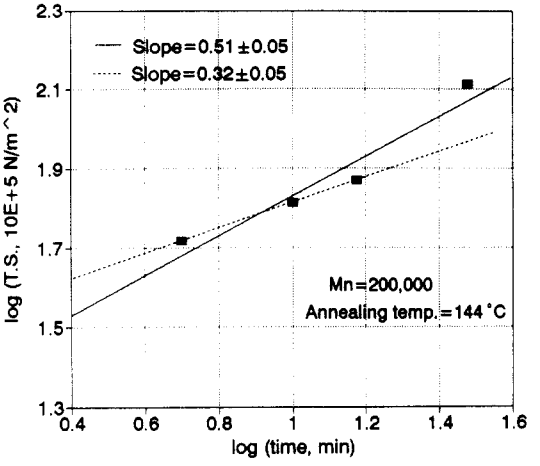

Figure 6. log–log plot showing the increase in tensile strength with annealing time.

observed that, after the tensile strength reaches its highest value, it drops and then recovers to a constant value. This feature was also observed in a study of the fracture energy and chain scission of latex films by Mohammadi et al.[38,39] and Yoo et al.[12,13] and is attributed to a change in the fracture mechanism from along the latex interfaces to straight through the material.

From the SANS data, the diffusion coefficient was calculated by using eq 14 or eq 15. The Q-constant diffusion coefficients obtained by the above analysis were 5.72×10^{-16}, 4.77×10^{-16}, and 3.78×10^{-16} cm²/s at Q = 0.0055, 0.0067, and 0.0077 Å^{-1}, respectively, all at 144 °C, with a time range of 0 min (just sintered) to 2 h.

In addition to the Q-constant diffusion coefficient, it would be quite valuable to determine diffusion coefficients at different annealing times over the entire Q range.

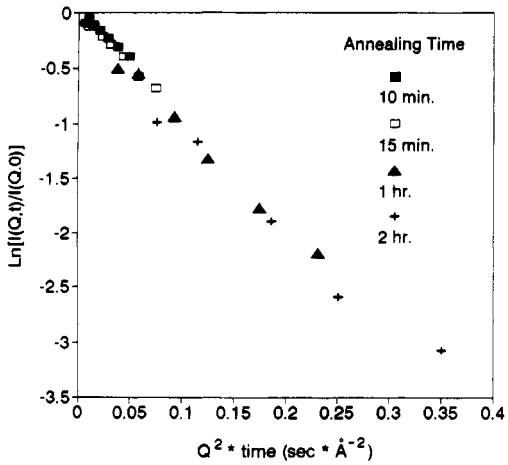

Figure 7. SANS data taken with the scattering angle, Q, for several annealing times (direct mini-emulsification system).

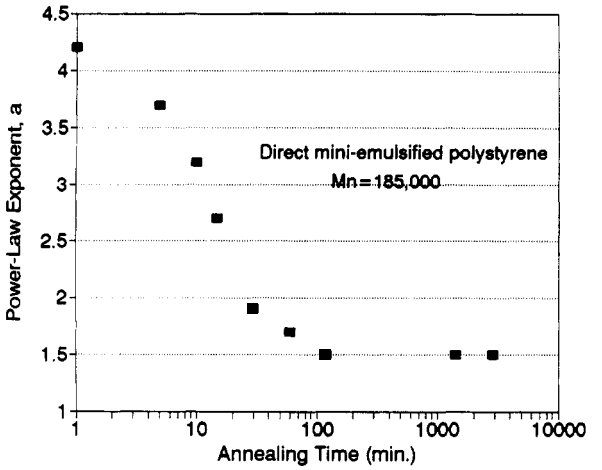

Figure 8. Power-law exponents as a function of annealing time.

Table IV. Diffusion Coefficients at Different Annealing Times

annealing time	D (10^{-16} cm^2/s)	annealing time	D (10^{-16} cm^2/s)
5 min	2.9	1 h	4.5
10 min	4.1	2 h	4.1
15 min	4.4	24 h	0.3
30 min	5.7	48 h	0.1

Diffusion coefficients are scattered at each Q value due to the instrumental resolution. The average D-value of each annealing time was obtained from a least-squares slope of $\ln[I(Q,t)/I(Q,0)]$ vs Q^2t plots at $0.003 \leq Q \leq 0.01$ Å^{-1} according to eq 14 as shown in Figure 7 and Table IV. As seen in Figure 7, data points show some deviation with increased annealing times; however, the extrapolated Q value must be zero by definition.

Fractal Analysis. The exponents of the power-law equation were obtained at different annealing times in the Porod region of the scattering intensity curve with the scattering angle. This portion of the curve can now be interpreted in terms of the fractal dimension. Figure 8 shows the variation of those exponents as a function of annealing time, a value at long times of 1.5 being obtained experimentally. At short annealing times, the power-law exponent is the Porod limit for a smooth sphere, and at long times the limit for the polymer solution in a good solvent should be $^5/_3$, and in polymer melts it should be 2.[34,37]

On the basis of eq 16, the following relations define the values of a:

a	interpretation
4	smooth sphere
3	rough sphere
2	Θ-solvent random coil or bulk materials[34]
$^5/_3$	athermal (good) solvent for random coils

Since Figure 8 shows long time values lower than these quantities, one is tempted to conclude the deuterated polymer is "well dissolved" in the protonated polymer. Table III shows that the radius of gyration is still high, suggesting the presence of some dimers and trimers.

Discussion

Diffusion Rate. As already pointed out in Figure 3, the direct mini-emulsification system has a much faster interdiffusion rate than the conventional emulsion polymerization system. Supporting this result, the present diffusion coefficient is compared with previously published results in Table V. Here, the previous data are converted to the present experimental conditions (M_n = 185 000 and temperature = 144 °C) by using the relationships of $D \propto M^{-2}$ and the WLF equation. Whereas Anderson and Jou[11] present a diffusion coefficient similar to that of the present system, the diffusion coefficient obtained by Yoo et al.[12,13] is almost 1 order of magnitude smaller than the two direct emulsified systems. The higher diffusion rate of the present system may be due to two reasons:

First, while the emulsion polymerized polystyrene contains significant numbers of ionic sulfate end groups, SO_4^{-2}, from the initiator potassium persulfate, the anionic polymerized polystyrene has a hydrogen atom on one end and a butyl group on the other end. The ionic end group is much larger in size, making diffusion slower than expected. Also, it is strongly hydrophilic, so that it is located on the particle surface in near contact with other SO_4^{-2} groups and so may need an additional driving force to counteract the polar attractive forces. This may result in slower initial chain interdiffusion during film annealing.

Second, since the conventional emulsion polymerized polystyrene has a broad molecular weight distribution and the diffusion coefficient is inversely proportional to the square of the molecular weight, the small chains may have diffused very rapidly in the Yoo et al.[12,13] system. This may yield uniform background of deuterated chains, which does not contribute to the scattering intensity. Thus, the smearing effect of the small molecules might cause the apparent diffusion coefficient to decrease during the SANS measurement. However, the difference in the diffusion rates is probably real, for the anionic polymers gained tensile strength more rapidly, as discussed below.

Tensile Strength Improvement. In Wool's theory[18,20,28] for crack healing at a polymer–polymer interface, the number of bridges intersecting an interface as a function of time is predicted by the minor chain reptation model. According to this theory, only the bridging chains create entanglements on both sides of the interface. These entanglements are most significant in determining the rheological and mechanical properties of the polymer. The most critical parameter in making a bridge is the critical entanglement molecular weight, M_c. Wool also described the polydispersity effect on the chain diffusion, that is, the contribution from the faster diffusing, shorter chains dominating the mechanical strength at short times, followed later by the slower diffusing longer chains.

The present sintering process cannot avoid a slight initial interdiffusion due to the high pressure and temperature. That gives rise to an initial tensile strength in the sintered sample. From Figure 4, the direct mini-emulsified system showed a higher tensile strength, especially at short times

Table V. Comparison of Diffusion Coefficients of Polystyrene Latex Films (Q = 0.0067 Å^{-1})

system	mol wt	annealing temp (°C)	diffusion coefficient (cm^2/s)	ref
direct emulsification	185 000 (M_w/M_n = 1.02)	144	4.77×10^{-16}	present work
emulsion polymerization	M_n = 69 000 M_w = 250 000	144	6.64×10^{-17} [a]	12
direct emulsification	68 000 (M_w/M_n = 1.02)	130	2.48×10^{-16} [a]	11

[a] Converted to M_n = 185 000 and 144 °C by $D \propto M^{-2}$ and the WLF equation.

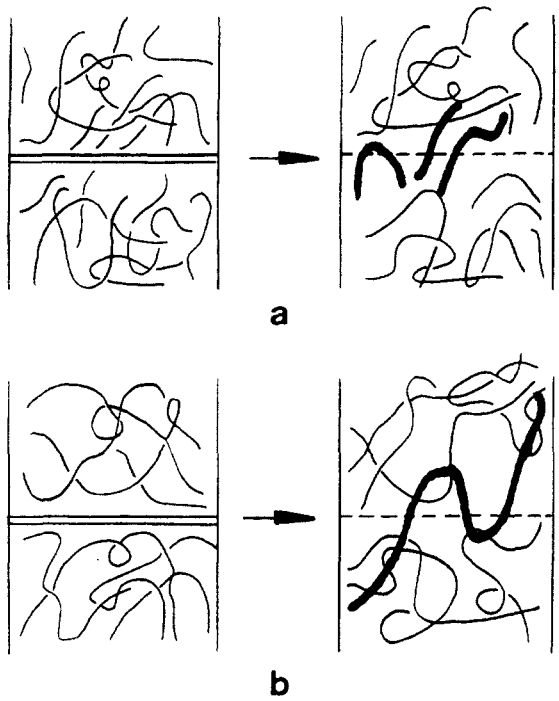

Figure 9. Description of polymer chain interdiffusion around the particle–particle interface at short annealing times: (a) broad chain length distribution (emulsion polymerized system), (b) narrow chain length distribution (direct mini-emulsified system).

in comparison with the conventional emulsion polymerized system. Since the emulsion polymerized polystyrene is composed of different chain lengths, the shortest chains are below the critical entanglement molecular weight, M_c = 32 000, for polystyrene. In this case, the short chains diffuse more quickly but cannot make multiple entanglements with neighboring polymer chains. However, a polymer with chain lengths greater than M_c can make entanglements with other chains during diffusion (see Figure 9) even if the diffusion rate is slower. Those few entanglements are believed to improve the mechanical strength of the film even at a short interdiffusion depth. This interpretation can be realized by measuring the number of bridges of both systems. Mohammadi et al.[39,40] recently showed that the tensile strength of partly annealed polystyrene latex films was proportional to the number of bridges formed.

As shown in Figure 5, the tensile strength has a maximum value and then it drops and levels off. Yoo et al.[12,13] and Mohammadi et al.[39,40] also observed similar maxima in tensile strength, and also in the number of chain scissions. The tensile strength of the latex film is governed by the chain bridge density at the particle–particle interface at the shorter annealing times. With increasing chain density of the interface due to the interdiffusion, the tensile strength increases also. However, there is a change in the fracture mechanism from through the particle–particle interfaces to through the particles. The shorter fracture path yields a decrease in the fracture energy and tensile strength.

Time Dependence of Tensile Strength Development. In Figure 6, the time-dependent tensile strength development is shown in a log–log plot. The experimental points, on a log–log scale, can be fitted to straight lines with slopes of 0.51 ± 0.05 and 0.32 ± 0.05. If only the first three points at early times are counted, then the power law is close to the one-fourth power rule. However, when all four points are used, the half power relationship is obtained. Which power-law exponent best represents the present system?

The Prager and Tirrell model[22-24] assumed that fracture toughness is related to the crossing density, σ, at the interface. This crossing density can be characterized for two cases, that is, equilibrium or uniform chain distribution at the initial interfaces and excess of chain ends at the initial interfaces. These two cases yield a half and one-fourth time dependence of the crossing density, respectively. In order to see the relationship between fracture toughness and the crossing density, Jud et al.[25] used the Griffith theory of fracture according to which crack initiation occurs when the stored elastic energy equals the energy required for the generation of the new crack surface. The elastic energy release follows the square of the applied stress, and the energy of the new crack surface is proportional to the chain crossing density in the case of a virgin linearly elastic polymer. Therefore, the fracture stress is dependent on the half power of the crossing density, $\sigma^{1/2}$. This then yields a fracture stress which is dependent on the one-fourth and a one-eighth power of the healing time. However, Prager and Tirrell argued that the fracture experiments of crack healing have not been made on virgin material but rather on material having a weakened region, and the fracture, especially at short healing times, is concentrated in this weakened region. On the basis of this argument, a more reasonable assumption is that the fracture stress should depend on σ rather than $\sigma^{1/2}$. Thus, in the case of healing of latex particle interfaces having a uniform chain end distribution as in the present system, the fracture stress is believed to follow the $^1/_2$ power law instead of $^1/_4$. This point has also been examined in another study on the polystyrene latex film formation having a narrow molecular weight distribution but different experimental conditions.[45]

Conclusions

A direct mini-emulsification method was used to make artificial latex particles having narrow molecular weight distribution and good particle size uniformity. The particles were cleaned, sintered, and partly annealed. The average depth of penetration of the polystyrene chains and tensile strength buildup were characterized during the course of film annealing.

Most interestingly, the direct mini-emulsified latex system has a greater interdiffusion rate and higher tensile strength at short annealing times than a corresponding conventional emulsion system at slightly lower molecular weights. The latter is believed to be significantly dom-

inated by the polydisperse nature of the molecular weight distribution and the larger and more polar chain end group. However, despite the different diffusion rates, both systems show a maximum in the tensile strength at a penetration depth comparable to 0.81 times the weight-average radius of gyration of the whole polystyrene chain as predicted by Wool. That is, half of the chain length, on average, is in the guest particle and half is in the host particle. Finally, the tensile strength data followed the half power time dependence.

Acknowledgment. The authors thank the National Science Foundation for support through Grant No. CBT-8820705. The SANS experiments were performed at the HFIR reactor in the Oak Ridge National Laboratory (ORNL). Research at Oak Ridge was supported in part by the Division of Materials Sciences, U.S. Department of Energy, under Contract No. DE-AC05-840R21400 with Martin Marietta Energy Systems, Inc., and also by the National Science Foundation.

References and Notes

(1) de Gennes, P.-G. *Macromolecules* **1976**, *9*, 587.
(2) Doi, M.; Edwards, S. F. *J. Chem. Soc., Faraday Trans. 2* **1978**, *74*, 1802.
(3) Klein, J. *Macromolecules* **1978**, *11*, 852.
(4) Graessley, W. W. *J. Polym. Sci., Polym. Phys. Ed.* **1980**, *18*, 27.
(5) Graessley, W. W. *Adv. Polym. Sci.* **1982**, *47*, 67.
(6) Tirrell, M. *Rubber Chem. Technol.* **1984**, *57*, 523.
(7) de Gennes, P.-G. *J. Chem. Phys.* **1971**, *55*, 572.
(8) Hahn, K.; Ley, G.; Schuller, H.; Oberthur, R. *Colloid Polym. Sci.* **1986**, *264*, 1092.
(9) Hahn, K.; Ley, G.; Oberthur, R. *Colloid Polym. Sci.* **1988**, *266*, 631.
(10) Linne, M. A.; Klein, A.; Miller, G. A.; Sperling, L. H.; Wignall, G. D. *J. Macromol. Sci., Phys.* **1988**, *B27* (2 & 3), 217.
(11) (a) Anderson, J. E.; Jou, J. H. *Macromolecules* **1987**, *20*, 1544. (b) Jou, J. H. Ph.D. Dissertation, The University of Michigan, Ann Arbor, MI, 1986.
(12) Yoo, J. N.; Sperling, L. H.; Glinka, C. J.; Klein, A. *Macromolecules* **1990**, *23*, 3962.
(13) Yoo, J. N.; Sperling, L. H.; Glinka, C. J.; Klein, A. *Macromolecules* **1991**, *24*, 2868.
(14) Pekcan, O.; Winnik, M. A.; Croucher, M. D. *Macromolecules* **1990**, *23*, 2673.
(15) Zhao, C. L.; Wang, Y.; Hruska, H.; Winnik, M. A. *Macromolecules* **1990**, *23*, 4082.
(16) Wang, Y.; Winnik, M. A. *Macromolecules* **1990**, *23*, 4731.
(17) Wool, R. P.; O'Connor, K. M. *J. Appl. Phys.* **1981**, *52*, 5194.
(18) Kim, Y. H.; Wool, R. P. *Macromolecules* **1983**, *16*, 1115.
(19) Zhang, H.; Wool, R. P. *Macromolecules* **1989**, *22*, 3018.
(20) Wool, R. P.; Yuan, B. L.; McGarel, O. *J. Polym. Eng. Sci.* **1989**, *29*, 1341.
(21) Whitlow, S. J.; Wool, R. P. *Macromolecules* **1991**, *24*, 5926.
(22) Prager, S.; Tirrell, M. *J. Chem. Phys.* **1981**, *75*, 5194.
(23) Prager, S.; Adolf, D.; Tirrell, M. *J. Chem. Phys.* **1983**, *78*, 7015.
(24) Prager, S.; Adolf, D.; Tirrell, M. *J. Chem. Phys.* **1986**, *84*, 5152.
(25) Jud, K.; Kausch, H. H.; Williams, J. G. *J. Mater. Sci.* **1981**, *16*, 204.
(26) Kumagai, Y.; Watanabe, H.; Miyasaka, K.; Hata, T. T. T. *Chem. Eng. Jpn.* **1979**, *12*, 1.
(27) Gilmore, P. T.; Falabella, R.; Lawrence, R. L. *Macromolecules* **1980**, *13*, 880.
(28) Wool, R. P. *J. Elastomers Plast.* **1985**, *17*, 106.
(29) Guinier, A.; Fournet, G. *Small Angle Scattering of X-rays*; John Wiley & Sons: New York, 1955.
(30) Binder, K. *J. Chem. Phys.* **1983**, *79*, 6387.
(31) Cook, H. *Acta Metall.* **1970**, *18*, 297.
(32) Summerfield, G. C.; Ullman, R. *Macromolecules* **1987**, *20*, 401.
(33) Summerfield, G. C.; Ullman, R. *Macromolecules* **1988**, *21*, 2643.
(34) Avnir, D. *The Fractal Approach to Heterogeneous Chemistry, Surfaces, Colloids, Polymers*; John Wiley & Sons: Chichester, U.K., 1989.
(35) Schaefer, D. W. *Mater. Res. Soc.* **1987**, *79*, 47.
(36) Schaefer, D. W.; Keefer, K. D. *Fractals in Physics*; North-Holland: Amsterdam, The Netherlands, 1985; p 39.
(37) Farnoux, B. Thesis, Université Louis Pasteur, Strasbourg, France, 1976.
(38) Mohammadi, N.; Kim, K. D.; Klein, A.; Sperling, L. H. *J. Colloid Interface Sci.* **1993**, *157*, 124.
(39) Mohammadi, N.; Yoo, J. N.; Klein, A.; Sperling, L. H. *J. Polym. Sci., Polym. Phys. Ed.* **1992**, *30*, 1311.
(40) Mohammadi, N.; Klein, A.; Sperling, L. H. *Macromolecules* **1993**, *26*, 1019.
(41) El-Aasser, M. S.; Misra, S. C.; Vanderhoff, J. W.; Manson, J. A. *J. Coat. Technol.* **1977**, *49*, 635.
(42) Vanderhoff, J. W.; El-Aasser, M. S.; Ugelstad, J. U.S. Patent 4,177,177, 1979.
(43) Tang, P. L. Ph.D. Dissertation, Lehigh University, Bethlehem, PA, 1991.
(44) Wignall, G. D.; Bates, F. S. *J. Appl. Crystallogr.* **1986**, *20*, 28.
(45) Kim, K. D.; Sperling, L. H.; Klein, A. submitted for publication in *Macromolecules*.